Three-dimensional converging–diverging Gaussian beam diffraction by a volume grating

Shun-Der Wu, Thomas K. Gaylord, Elias N. Glytsis,* and Yu-Ming Wu

*School of Electrical and Computer Engineering and Microelectronics Research Center,
Georgia Institute of Technology, Atlanta, Georgia 30332*

The diffraction characteristics of a volume grating (VG) illuminated by a three-dimensional (3-D) converging–diverging Gaussian beam at conical incidence are investigated by applying 3-D finite-beam (FB) rigorous coupled-wave analysis (RCWA) based on the conventional 3-D RCWA in conjunction with two-dimensional plane-wave decomposition. The Gaussian beam is assumed to have an arbitrary incidence angle, an arbitrary azimuthal angle, and any linear polarization. The two cases with linear polarizations of the central beam of the Gaussian ($\mathbf{E} \perp \mathbf{K}$ and $\mathbf{H} \perp \mathbf{K}$) are investigated. The diffraction efficiencies and the diffracted beam profiles for both unslanted VGs and slanted VGs (designed for substrate-mode optical interconnects) are presented. In general, the diffraction efficiencies of a converging–diverging spherical Gaussian beam diffracted by both unslanted VGs and slanted VGs increase and approach the central-beam results as the refractive-index modulation increases. © 2005 Optical Society of America

OCIS codes: 050.0050, 050.1950, 050.1960, 050.7330, 260.2110.

1. INTRODUCTION

In recent years optical interconnects have been considered a promising technology capable of supporting the interconnection requirements of future gigascale integration systems. For the implementation of optical interconnects, diffractive optics is a particularly promising technology. For example, diffractive optical elements, such as volume gratings (VGs) and surface-relief gratings (SRGs), can be used to couple an optical signal into (or out of) a substrate as a substrate-mode optical interconnect[1,2] and into (or out of) a waveguide as a guided-wave optical interconnect.[3–7] However, for practical applications the incident beam emitted by a single-mode optical fiber or a single-mode laser closely approximates a three-dimensional (3-D) converging–diverging spherical Gaussian beam. In addition, the incident wave vector may not lie in the plane perpendicular to the grating surface that contains the grating vector, and therefore it gives rise to 3-D conical diffraction.

To analyze 3-D conical diffraction, Chuang and Kong[8] first applied the integral method by using a Green's function approach to analyze a SRG with a small groove depth of 0.3 of the grating period. Moharam and co-workers[9,10] proposed a 3-D rigorous coupled-wave analysis (RCWA) to study the diffraction efficiencies of a planar VG with respect to the grating thickness and the incident angle and the diffraction efficiencies of a binary grating with respect to the normalized groove depth. Popov and Mashev[11] applied a rigorous differential method to investigate the conical diffraction of both a nonperfectly conducting SRG and a dielectric SRG. Gupta[12] utilized the Rayleigh method to study the characteristics of surface-plasmon excitation on an Ag SRG in conical diffraction with respect to the grating thickness and the azimuthal angle. Depine[13] and Gigli and Depine[14] applied both the conformal mapping method and the Rayleigh method to inves-

tigate the diffraction characteristics for a finitely conducting SRG and for a corrugated interface between an isotropic medium and a uniaxial crystal in a conical geometry, respectively. Furthermore, Abe and Koshiba[15] applied a differential method to investigate the effects of normalized groove depth, free-space wavelength, incident angle, and azimuthal angle on the diffraction efficiencies of 3-D conical diffraction by a SRG. Cornet *et al.*[16] applied a similar differential method to analyze 3-D conical diffraction of a plane wave by an inclined parallel-plate grating for a variety of incident angles and azimuthal angles. More recently, Ohki *et al.*[17] applied the transition-matrix method to analyze electromagnetic wave diffraction from a sinusoidal SRG for arbitrary angles of incidence and polarization. However, in all of these analyses, the incident beam was assumed to be a plane wave.

On the other hand, for the incidence of a Gaussian beam, depending on the two-dimensional (2-D) (cylindrical) or 3-D (spherical) profile and the phase curvature of an incident beam, the Gaussian beam can be classified into four categories: the 2-D Gaussian-profile plane wave (neglecting the phase curvature of the beam), the converging–diverging cylindrical Gaussian beam, the 3-D Gaussian-profile plane wave, and the converging–diverging spherical Gaussian beam. For the diffraction analysis of a grating illuminated by a 2-D Gaussian-profile plane wave, Moharam *et al.*[18] applied a 2-D coupled-wave analysis (CWA) to analyze the diffraction of finite beams by planar VGs in the Bragg-diffraction regime (i.e., only the transmitted beam and diffracted beam were considered). The diffraction efficiencies and the profiles of the transmitted beam and the diffracted beam as functions of the grating strength and the geometry parameter were presented. Notni and Kowarschik[19] used the same CWA to study the diffraction characteristics of an absorption VG. Also, Boffi *et al.*[20] investigated the dis-

tortions of the transmitted beam and the diffracted beam both theoretically by use of the CWA and the beam propagation method and experimentally by use of a LiNbO$_3$ VG read out by a 1550-nm Gaussian beam.

For the converging–diverging cylindrical Gaussian beam incident on a grating, Chu and Tamir[21,22] utilized guided-wave analysis in conjunction with plane-wave decomposition (PWD) to study the diffraction of Gaussian beams by periodically modulated media for both on-Bragg and off-Bragg incidences in the Bragg-diffraction regime. The beam-splitting phenomenon inside the modulated region was presented. Benlarbi *et al.*[23,24] used both Raman–Nath analysis and the 2-D CWA in conjunction with PWD to investigate the case of Bragg diffraction of a Gaussian beam by an unslanted VG. In addition, Kriezis *et al.*[25] applied the method of moments with PWD to analyze the diffraction of a converging–diverging cylindrical Gaussian beam from a periodic planar screen of perfectly conducting strips. McNeill and Poon[26] adopted the multiple-plane-wave scattering theory (based on Fourier transform theory and the plane-wave transfer function) to study the effects of the beam width and the grating thickness on the diffracted-beam distortion by an acoustic grating. In general, the narrower the incident beam and the thicker the grating, the more severe is the distortion of the diffracted beam. However, this multiple-plane-wave scattering formalism was derived based on the Raman–Nath equation, and therefore this method is restricted to the scalar diffraction regime. Moreover, Skigin and Depine[27] proposed a multilayer modal analysis with PWD to analyze the diffraction from SRGs with sinusoidal, triangular, and rectangular profiles. Recently, Mata-Mendez and Chavez-Rivas[28] and Sumaya-Martines *et al.*[29] applied both Rayleigh–Sommerfeld theory and modal analysis in conjunction with PWD to study the diffraction of a Gaussian beam by a lamellar grating in both the scalar diffraction regime and the vectorial diffraction regime, respectively.

In contrast to the cylindrical (2-D) Gaussian beam, Siegman[30] and Hamad and Wicksted[31] applied the Green's function integral to solve the paraxial wave equation for studying the diffraction efficiencies of a crossed-beam VG illuminated by a spherical (3-D) Gaussian beam. The effects of the beam size and the incidence angle on diffraction efficiencies were presented. Furthermore, Moharam *et al.*[32] applied the CWA to investigate the diffraction characteristics, including diffraction efficiencies and diffracted-beam profile, as a function of grating strength for a crossed-beam VG with a spherical Gaussian-beam incidence. Recently Wang[33] proposed an impulse-response technique in conjunction with the CWA to study the propagation and diffraction of a spherical Gaussian beam in a planar VG. The beam distortion could be observed for a grating with a higher grating-thickness-to-beam-width ratio. However, all 3-D Gaussian beams treated in these analyses were assumed to be 3-D Gaussian-profile plane waves, and all diffraction analyses were restricted to the Bragg-diffraction regime. On the other hand, Landry and Maldonado[34] applied the 4×4 matrix method in conjunction with PWD to investigate the transmission and the reflection of a converging–diverging spherical Gaussian beam from an anisotropic

multilayer structure instead of from a periodic medium (i.e., a grating).

Although a variety of numerical methods have been applied to analyze the diffraction of both cylindrical (2-D) Gaussian beams and spherical (3-D) Gaussian beams by gratings, they focused only on the classical diffraction geometry (i.e., the grating vector was restricted to lie in the incident plane). To the authors' knowledge, there is no paper that treats the realistic situation of a grating illuminated by a converging–diverging spherical Gaussian beam at conical incidence. Therefore in this paper the 3-D finite-beam (FB) RCWA derived from the conventional 3-D RCWA[9,10] in conjunction with PWD is applied to investigate the diffraction characteristics of a planar VG illuminated by a converging–diverging spherical Gaussian beam at conical incidence. The Gaussian beam with any incident angle, any azimuthal angle, and any linear polarization orientation is assumed to be focused on the input surface of a planar VG. In Section 2 the numerical method is briefly introduced. In Section 3 the numerical results for diffraction efficiencies and beam profiles for both unslanted VGs and slanted VGs (that are designed for substrate-mode optical interconnects) are presented. The two cases with linear polarizations of the central beam of the Gaussian ($\mathbf{E} \perp \mathbf{K}$ and $\mathbf{H} \perp \mathbf{K}$) are investigated. Finally, the primary results are summarized in Section 4.

2. ANALYSIS METHOD

A. Configuration
The general configuration for 3-D diffraction by a planar VG of thickness d is shown in Fig. 1. The VG consists of a periodic variation in the optical frequency dielectric constant with a period Λ and a slant angle ϕ_g throughout the volume of the grating. The grating vector $\mathbf{K}$ is defined as $\mathbf{K} = |\mathbf{K}|(\hat{x} \sin \phi_g + \hat{z} \cos \phi_g)$, where $|\mathbf{K}| = 2\pi/\Lambda$ and $\hat{x}$, $\hat{z}$ are the unit vectors along the x and z directions, respectively. The optical frequency dielectric constant in the grating region can be written as
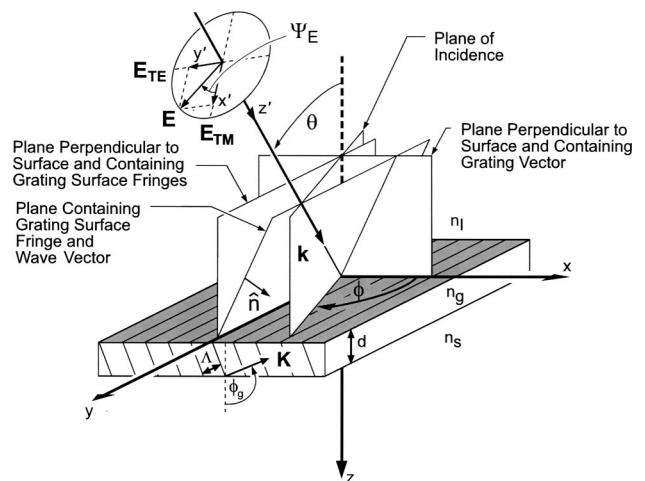

Fig. 1.   Geometry of a planar VG illuminated by a converging–diverging spherical Gaussian beam with wave vector $\mathbf{k}$ at an arbitrary incidence angle θ, at an arbitrary azimuthal angle ϕ, and with an arbitrary linear polarization (specified by the polarization angle Ψ_E). The VG has period Λ, slant angle ϕ_g, and thickness d. The refractive indices of the incident region, the grating, and the substrate are n_I, n_g, and n_s, respectively.

$$\epsilon = \epsilon_0 + \sum_{p=1}^{\infty} \epsilon_p^c \cos(p\mathbf{K} \cdot \mathbf{r}) + \sum_{p=1}^{\infty} \epsilon_p^s \sin(p\mathbf{K} \cdot \mathbf{r}), \qquad (1)$$

where $\epsilon_0 = n_g^2$ is the average optical frequency dielectric constant, ϵ_p^c and ϵ_p^s are the pth harmonics of the optical frequency dielectric constant (all in the grating region), and $\mathbf{r}$ is the position vector ($\mathbf{r} = x\hat{x} + z\hat{z}$).

In addition, a converging–diverging spherical Gaussian beam with any linear polarization orientation specified by the polarization angle Ψ_E propagates along the $\mathbf{z}'$ direction [in the beam-coordinate system (x',y',z')] and is obliquely incident at an arbitrary incidence angle θ and at an arbitrary azimuthal angle ϕ [in the VG coordinate system (x,y,z)] from the incident region with refractive index n_I upon a planar VG and then diffracts into the substrate region with refractive index n_s as a substrate-mode optical interconnect. On the basis of the beam-coordinate system (x',y',z'), the converging–diverging spherical Gaussian beam (assumed to be focused on the input surface of a planar VG) can be represented as

$$\mathbf{E}^{\text{inc}} = \left[\frac{w_{0x'}}{w_{x'}(z')}\right]^{1/2} \left[\frac{w_{0y'}}{w_{y'}(z')}\right]^{1/2} \exp\left\{-\left[\left(\frac{x'}{w_{x'}(z')}\right)^2\right.\right.$$

$$\left.\left. + \left(\frac{y'}{w_{y'}(z')}\right)^2\right]\right\} \exp\left\{-j\frac{1}{2}k\left[\frac{x'^2}{R_{x'}(z')} + \frac{y'^2}{R_{y'}(z')}\right]\right\}$$

$$\times \exp\left\{j\frac{1}{2}\left[\tan^{-1}\left(\frac{z'}{z_{0x'}}\right) + \tan^{-1}\left(\frac{z'}{z_{0y'}}\right)\right]\right\}$$

$$\times \exp(-jkz')\hat{e} = E^{\text{inc}}\hat{e}, \qquad (2)$$

where $w_{0u'}$ is the beam radius at the beam waist (that is located at $z'=0$) in the u' ($u'=x'$ or $u'=y'$) direction, $k = k_0 n_I = (2\pi/\lambda_0)n_I$ is the wave number of the incident beam, and λ_0 is the free-space wavelength. The beam radius $w_{u'}(z')$, the radius of curvature of the phase front of the beam $R_{u'}$, and the Rayleigh range $z_{0u'}$ in the u' direction are

$$w_{u'}(z') = w_{0u'}\left[1 + \left(\frac{z'}{z_{0u'}}\right)^2\right]^{1/2}, \qquad (3)$$

$$R_{u'}(z') = z'\left[1 + \left(\frac{z_{0u'}}{z'}\right)^2\right], \qquad (4)$$

$$z_{0u'} = \frac{\pi n_I}{\lambda_0}w_{0u'}^2. \qquad (5)$$

In addition, $\hat{e}$ is the polarization unit vector of the central beam given by

$$\hat{e} = e_x\hat{x} + e_y\hat{y} + e_z\hat{z} = (\cos\Psi_E \cos\phi \cos\theta - \sin\Psi_E \sin\phi)\hat{x}$$

$$+ (\cos\Psi_E \sin\phi \cos\theta + \sin\Psi_E \cos\phi)\hat{y} + (\cos\Psi_E \sin\theta)\hat{z}. \qquad (6)$$

The corresponding configuration of a converging–diverging spherical Gaussian beam focused on the input surface of a planar grating at an arbitrary incidence angle and at zero azimuthal angle ($\phi=0°$) on the $x-z$ plane is shown in Fig. 2. The two cases with linear polarizations of

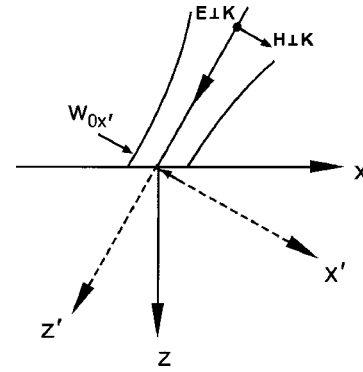Fig. 2. Configuration of a converging–diverging spherical Gaussian beam at an arbitrary incidence angle θ and at zero azimuthal angle $\phi=0°$ on the $x-z$ plane. $w_{0x'}$ is the beam radius of the incident beam at the beam waist along the x' direction. The two cases with linear polarizations of the central beam of the Gaussian of $\mathbf{E} \perp \mathbf{K}$ and $\mathbf{H} \perp \mathbf{K}$ corresponding to the polarization angles $\Psi_E=90°$ and $\Psi_E=0°$, respectively, are presented.

the central beam of the Gaussian of $\mathbf{E} \perp \mathbf{K}$ (i.e., the electric-field vector is perpendicular to the $x-z$ plane, and thus $\Psi_E=90°$) and $\mathbf{H} \perp \mathbf{K}$ (i.e., the magnetic-field vector is perpendicular to the $x-z$ plane, and thus $\Psi_E=0°$) investigated in this paper are also presented.

B. Three-Dimensional Finite-Beam Rigorous Coupled-Wave Analysis

The conventional 3-D RCWA[9,10] is perhaps the most common method applied to analyze rigorously the 3-D conical diffraction by a grating. However, this conventional 3-D RCWA has an important assumption that the incident beam is a plane wave. Therefore, for the rigorous analysis of a converging–diverging spherical Gaussian beam incident upon a grating, a method referred to as the 3-D FB RCWA is developed in this paper. The first step of 3-D FB RCWA is to determine the plane-wave spectrum of the incident beam by applying a 2-D discrete Fourier transform. This step is also referred to as 2-D PWD. A discrete transform is applied rather than an integral formalism because the incident electric field is represented as a discrete set of plane waves. Furthermore, the discrete transform is much better suited for numerical implementation on a digital computer. For each subbeam (i.e., each propagating component of the plane-wave spectrum) specified by an incident angle, an azimuthal angle, a polarization angle, and a plane-wave spectrum coefficient, the conventional 3-D RCWA provides the reflection vectors, the transmission vectors, and diffraction efficiencies of the various diffracted orders. Coherently combining the conventional 3-D RCWA results for all subbeams can yield the diffracted fields and diffraction efficiencies of the various diffracted orders.

1. Two-Dimensional Plane-Wave Decomposition
Applying the 2-D discrete Fourier transform allows the incident-field amplitude at $z=0$ (i.e., the interface between the grating and the incident region) to be expanded in terms of its plane-wave spectrum as

$$E^{\text{inc}}(x,y,z=0) = \sum_{m_x=-M_x/2}^{M_x/2-1} \sum_{m_y=-M_y/2}^{M_y/2-1} F(k_{x,m_x},k_{y,m_y})$$
$$\times \exp[-j(k_{x,m_x}x + k_{y,m_y}y)], \qquad (7)$$

where M_u is the number of sampling points over the interval $-L_u/2 \leqslant u \leqslant L_u/2$ and $k_{u,m_u} = m_u(2\pi/L_u)$ is the wave vector component along the u ($u=x$ or y) direction. As a result, the z wave vector component for the (m_x,m_y) subbeam in the incident region can be written as $k_{z,m_x,m_y} = (k_0^2 n_I^2 - k_{x,m_x}^2 - k_{y,m_y}^2)^{1/2}$. In addition, the corresponding plane-wave spectrum coefficient $F(k_{x,m_x},k_{y,m_y})$ for the (m_x,m_y) subbeam can be determined by

$$F(k_{x,m_x},k_{y,m_y}) = \frac{1}{M_x M_y} \sum_{n_x=-M_x/2}^{M_x/2-1} \sum_{n_y=-M_y/2}^{M_y/2-1} E^{\text{inc}}(x_n,y_n,z=0)$$
$$\times \exp[j(k_{x,m_x}x_n + k_{y,m_y}y_n)], \qquad (8)$$

where $x_n = n_x L_x/M_x$ and $y_n = n_y L_y/M_y$. Therefore, for the (m_x,m_y) subbeam, the incidence angle θ_{m_x,m_y} and the azimuthal angle ϕ_{m_x,m_y} in the incident region can be determined, respectively, by

$$\theta_{m_x,m_y} = \cos^{-1}\left(\frac{k_{z,m_x,m_y}}{k_0 n_I}\right), \qquad (9)$$

$$\phi_{m_x,m_y} = \tan^{-1}\left(\frac{k_{y,m_y}}{k_{x,m_x}}\right). \qquad (10)$$

Since the incident Gaussian beam is assumed to be a linearly polarized light, which can be realized by use of a polarizer, the polarization unit vector of each subbeam $\hat{e}_{m_x,m_y}$ is located at the intersection of two planes. The first plane is referred to as the plane of polarization and consists of the polarization unit vector of the central beam $\hat{e}$ and the wave vector of the incident beam $\mathbf{k}$. The second plane is the plane that is normal to the wave vector of the (m_x,m_y) subbeam $\mathbf{k}_{m_x,m_y} = k_{x,m_x}\hat{x} + k_{y,m_y}\hat{y} + k_{z,m_x,m_y}\hat{z}$ (i.e., the constant-phase plane of a specific subbeam). Applying fundamental calculations in geometry, including both inner product and cross product of two vectors, the polarization angle of the (m_x,m_y) subbeam, Ψ_{E,m_x,m_y}, can be easily derived as

$$\Psi_{E,m_x,m_y} = \cos^{-1}(\hat{e}_{\text{TM}} \cdot \hat{e}_{m_x,m_y}) \frac{(\hat{e}_{\text{TM}} \times \hat{e}_{m_x,m_y}) \cdot \mathbf{k}}{|\hat{e}_{\text{TM}} \times \hat{e}_{m_x,m_y}||\mathbf{k}|}, \qquad (11)$$

where $\hat{e}_{\text{TM}}$ is the unit vector of $\mathbf{E}_{\text{TM}}$ (as shown in Fig. 1) and $\hat{e}_{m_x,m_y}$ is given by

$$\hat{e}_{m_x,m_y} = \frac{(\hat{k} \times \hat{e}) \times \hat{k}_{m_x,m_y}}{|(\hat{k} \times \hat{e}) \times \hat{k}_{m_x,m_y}|}, \qquad (12)$$

where $\hat{k} = \mathbf{k}/|\mathbf{k}|$ and $\hat{k}_{m_x,m_y} = \mathbf{k}_{m_x,m_y}/|\mathbf{k}_{m_x,m_y}|$.

2. Diffracted Fields and Diffraction Efficiencies
With the above procedure, the incident beam of a converging–diverging spherical Gaussian beam has been rewritten in terms of its plane-wave spectrum, each sub-

beam of which is specified by an incident angle θ_{m_x,m_y}, an azimuthal angle ϕ_{m_x,m_y}, a polarization angle Ψ_{E,m_x,m_y}, and a plane-wave spectrum coefficient $F(k_{x,m_x},k_{y,m_y})$, but no interaction with the grating has been considered. Therefore, in order to model rigorously the interaction of a converging–diverging spherical Gaussian beam with a planar VG, the conventional 3-D RCWA[9,10] is applied to each subbeam. For each subbeam the conventional 3-D RCWA solution provides both the reflection vector $\mathbf{R}_{m_x,m_y,i}$ and the transmission vector $\mathbf{T}_{m_x,m_y,i}$, where the index i indicates the ith diffracted order. As a result, the reflected electric field $\mathbf{E}^R(x,y,z)$ in the incident region and the transmitted electric field $\mathbf{E}^T(x,y,z)$ in the substrate region can be respectively expressed as a coherent sum over all subbeams and all diffracted orders as

$$\mathbf{E}^R(x,y,z) = \sum_i \sum_{m_x=-M_x/2}^{M_x/2-1} \sum_{m_y=-M_x/2}^{M_y/2-1} F(k_{x,m_x},k_{y,m_y})\mathbf{R}_{m_x,m_y,i}$$
$$\times \exp[-j(k_{x,m_x,i}x + k_{y,m_y,i}y + k_{z,m_x,m_y,i}^R z)], \qquad (13)$$

$$\mathbf{E}^T(x,y,z) = \sum_i \sum_{m_x=-M_x/2}^{M_x/2-1} \sum_{m_y=-M_y/2}^{M_y/2-1} F(k_{x,m_x},k_{y,m_y})\mathbf{T}_{m_x,m_y,i}$$
$$\times \exp\{-j[k_{x,m_x,i}x + k_{y,m_y,i}y + k_{z,m_x,m_y,i}^T(z-d)]\}, \qquad (14)$$

where $k_{x,m_x,i} = k_{m_x} - i|\mathbf{K}|\sin\phi_g$ and $k_{y,m_y,i} = k_{m_y}$. In addition, the quantities of $k_{z,m_x,m_y,i}^R$ and $k_{z,m_x,m_y,i}^T$ can be respectively represented as

$k_{z,m_x,m_y,i}^R$

$$= \begin{cases} -(k_0^2 n_I^2 - k_{x,m_x,i}^2 - k_{y,m_y,i}^2)^{1/2} & \text{for propagation} \\ \qquad\qquad \text{waves} \\ +j(k_{x,m_x,i}^2 + k_{y,m_y,i}^2 - k_0^2 n_I^2)^{1/2} & \text{for evanescent} \\ \qquad\qquad \text{waves} \end{cases}, \qquad (15)$$

$k_{z,m_x,m_y,i}^T$

$$= \begin{cases} +(k_0^2 n_s^2 - k_{x,m_x,i}^2 - k_{y,m_y,i}^2)^{1/2} & \text{for propagation} \\ \qquad\qquad \text{waves} \\ -j(k_{x,m_x,i}^2 + k_{y,m_y,i}^2 - k_0^2 n_s^2)^{1/2} & \text{for evanescent} . \\ \qquad\qquad \text{waves} \end{cases}. \qquad (16)$$

Furthermore, applying the Poynting theory and neglecting the interference between various diffracted orders of two different subbeams of the incident beam, the diffraction efficiency for the ith diffracted order can be easily derived as

$$\mathrm{DE}_i^l = \frac{P_i^l}{P^{\mathrm{inc}}}$$

$$= \frac{\displaystyle\sum_{m_x}\sum_{m_y} |F(k_{x,m_x}, k_{y,m_y})|^2 \, \mathrm{Re}(k_{z,m_x,m_y}^*)\mathrm{DE}_{m_x,m_y,i}^l}{\displaystyle\sum_{m_x}\sum_{m_y} |F(k_{x,m_x}, k_{y,m_y})|^2 \, \mathrm{Re}(k_{z,m_x,m_y}^*)},$$

$$(l = R, T), \quad (17)$$

where P^{inc} is the power of the incident beam, P_i^l is the power of the ith diffracted order ($l = R$ for backward and $l = T$ for forward), $\mathrm{DE}_{m_x,m_y,i}^l$ is the diffraction efficiency of the ith backward-diffracted ($l = R$) order or the ith forward-diffracted ($l = T$) order for the (m_x, m_y) subbeam (that is determined by the conventional 3-D RCWA), and Re( ) denotes the real part of a complex number.

3. RESULTS

For all the cases that are investigated in this paper, a linearly polarized converging–diverging spherical Gaussian beam with beam radius $w_{0x'} = w_{0y'} = 2$ μm (at the beam waist) for both the central-beam $\mathbf{E} \perp \mathbf{K}$ polarization case and the central-beam $\mathbf{H} \perp \mathbf{K}$ polarization case focused on the VG (Fig. 2) is considered. The free-space wavelength of the incident beam is assumed to be $\lambda_0 = 850$ nm (e.g., a GaAs laser). Moreover, for all calculations in this paper, the Gaussian beam is decomposed into 14,400 (i.e., $M_x = M_y = 120$) propagating plane waves by use of 2-D PWD (as described in Subsection 2.B.1). On the other hand, the VG analyzed in this paper comprises an incident region of air with refractive index $n_I = 1.0$ and a substrate with refractive index $n_s = 1.55$ (e.g., benzocyclobutane, BCB). The grating material is a photopolymer with average dielectric constant $\epsilon_0 = 2.25$ ($n_g = 1.5$) (e.g., DuPont's Omni-Dex613 photopolymer). In addition, the grating thickness is assumed to be $d = 10$ μm. Both an unslanted VG and a slanted VG are investigated in this paper. It is noted that the slanted VG analyzed in this paper is designed for a substrate-mode optical interconnect, as the incident beam is normally incident on the VG.

A. Unslanted Volume Gratings
For the case of an unslanted VG, the grating period is selected as the same as the free-space wavelength $\Lambda = \lambda_0 = 850$ nm, and the slant angle is $\phi_g = 90°$. To satisfy the first-order Bragg condition of the central subbeam of the incident beam, the incident angle and the azimuthal angle are designed as $\theta = 30°$ and $\phi = 0°$, respectively.

1. $\mathbf{E} \perp \mathbf{K}$ Polarization
Figure 3 shows the diffraction efficiencies of the −1st forward-diffracted order, DE_{-1}^T, for the converging–diverging spherical Gaussian beam and its corresponding five major subbeams (including the central subbeam, the $\pm k_x/e$ subbeams, and the $\pm k_y/e$ subbeams) as a function of the refractive-index modulation, Δn_1. The definitions of the central subbeam, the $\pm k_x/e$ subbeams, and the $\pm k_y/e$ subbeams of a converging–diverging spherical Gaussian beam can be found in Appendix A. As shown is in Fig. 3(a),

the period of the variation of DE_{-1}^T with respect to Δn_1 is $\Delta n_1^p = 0.08$, which is close to the value determined by Kogelnik's analysis[35]:

$$\Delta n_1^p = \frac{\lambda_0 \sqrt{C_R C_S}}{d(\hat{r}_E \cdot \hat{s}_E)}, \quad (18)$$

where $C_R = \cos\theta_{\mathrm{ins}}$, $C_S = \cos\theta_{\mathrm{ins}} + (\lambda_0/n_g)\cos\phi_g/\Lambda$, $\theta_{\mathrm{ins}} = 19.47°$ is the incident angle inside the grating, and $\hat{r}_E \cdot \hat{s}_E = \cos 90° = 1$ is the inner product of two unit polarization vectors of the 0th and the −1st forward-diffracted fields, respectively.

Comparing the diffraction efficiency of the converging–diverging spherical Gaussian beam [Fig. 3(a)] to that of the central subbeam corresponding to the response of a plane-wave incidence [solid curve in Fig. 3(b)], the diffraction efficiency of the Gaussian beam increases and approaches the central-beam result. For example, for $\Delta n_1 = 0.02$, the diffraction efficiencies are $\mathrm{DE}_{-1}^T = 0.2802$ and $\mathrm{DE}_{-1}^T = 0.4642$ for the Gaussian beam and its corresponding central beam, respectively. However, for a sufficiently large refractive-index modulation, such as $\Delta n_1 = 0.12$, the diffraction efficiency of the converging–diverging spherical Gaussian beam is $\mathrm{DE}_{-1}^T = 0.7814$, approaching to that
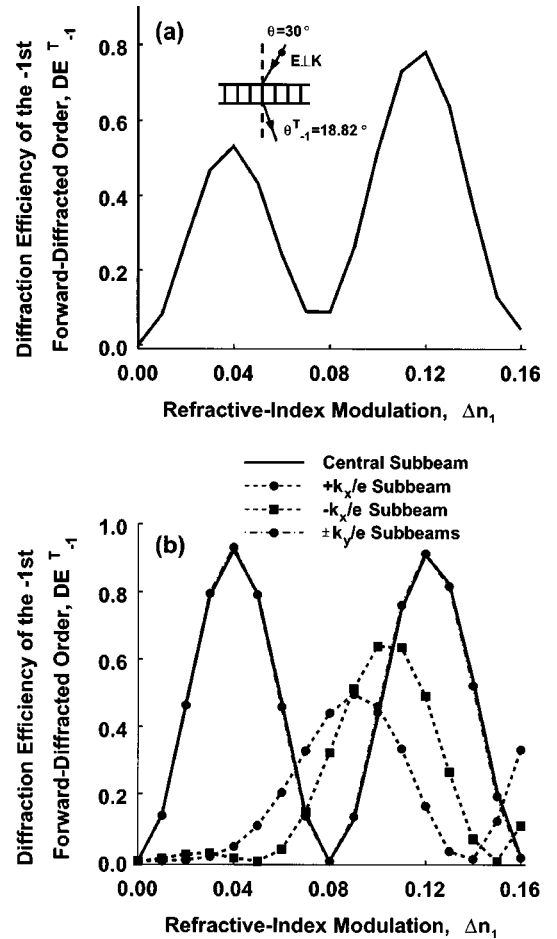

Fig. 3. Diffraction efficiencies of the −1st forward-diffracted order of an unslanted VG for (a) a converging–diverging spherical Gaussian beam and (b) its corresponding five major subbeams as a function of the refractive-index modulation for the central-beam $\mathbf{E} \perp \mathbf{K}$ polarization case.
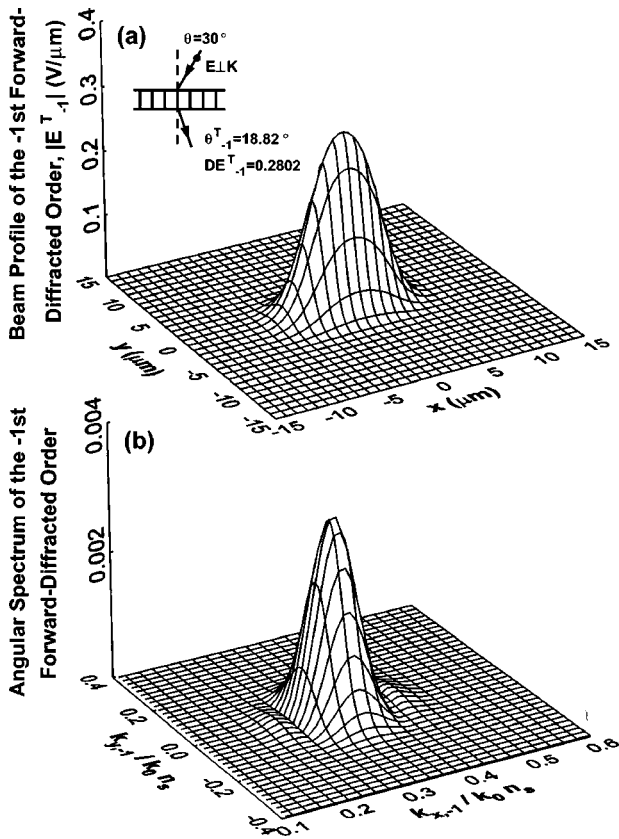
Fig. 4. (a) 3-D beam profile at $z = 10$ μm and (b) its corresponding angular spectrum of the −1st forward-diffracted order of an unslanted VG for the central-beam $\mathbf{E} \perp \mathbf{K}$ polarization case with grating $\Delta n_1 = 0.02$.

of the central beam ($\mathrm{DE}^T_{-1} = 0.9112$). This characteristic of the effect of Δn_1 on the diffraction efficiency of a converging–diverging spherical Gaussian is in agreement with that of a 2-D Gaussian-profile plane wave.[18] In addition, as is shown in Fig. 3(b), for small refractive-index modulations ($\Delta n_1 \lesssim 0.03$) the diffraction efficiencies for both $\pm k_x/e$ subbeams are much smaller than those of the central subbeam (satisfied Bragg condition), because these two subbeams move away from the Bragg condition, and therefore result in small diffraction efficiencies. However, as the refractive-index modulation increases, the diffraction efficiencies of both $\pm k_x/e$ subbeams increase and become comparable with those of the central subbeam. In contrast to the $\pm k_x/e$ subbeams, the diffraction efficiencies of both $\pm k_y/e$ subbeams are close to satisfying the Bragg condition. It is also noted that the diffraction efficiencies of the $+k_y/e$ subbeam and the $-k_y/e$ subbeam are identical. This result is expected, since these two subbeam/grating configurations are equivalent.

Figure 4 shows the 3-D beam profile at $z = 10$ μm (i.e., the interface between the VG and the substrate) and its corresponding angular spectrum of the −1st forward-diffracted order for the central-beam $\mathbf{E} \perp \mathbf{K}$ polarization case as the refractive-index modulation is $\Delta n_1 = 0.02$ (based on DuPont's OmniDex613 photopolymer).[36,37] As is shown in Fig. 4(a), the beam profile of the −1st forward-diffracted order is no longer Gaussian; i.e., the converging–diverging spherical Gaussian beam is dis-

torted by the VG. On the other hand, as is shown in Fig. 4(b), the angular spectrum of the −1st forward-diffracted order is centered at the components of the normalized wave vector of $k_{x,-1}/k_0 n_s = 0.323$ and $k_{y,-1}/k_0 n_s = 0$. In other words, the diffracted angle of the −1st propagating order in the substrate is $\theta^T_{-1} = 18.82°$ (measured from $+z$ axis in a counterclockwise direction) on the x–z plane, which is equal to the value determined by the simple grating equation. Furthermore, the corresponding diffraction efficiency is 28.02%. It is also worth mentioning that the subbeams with $k_{y,-1} = 0$ and the subbeams with $k_{y,-1} \neq 0$ of the −1st forward-diffracted beam are linearly polarized and elliptically polarized, respectively.

2. $\mathbf{H} \perp \mathbf{K}$ *Polarization*

For the central-beam $\mathbf{H} \perp \mathbf{K}$ polarization case, the diffraction efficiencies DE^T_{-1} for the converging–diverging spherical Gaussian beam and its corresponding five major subbeams as a function of Δn_1 are presented in Fig. 5. As is shown in Fig. 5(a), the period of the variation of DE^T_{-1} with respect to Δn_1 is $\Delta n^p_1 = 0.10$, which is close the value determined by Kogelnik's analysis [estimated by Eq. (18) for $\theta_{\text{ins}} = 19.47°$ and $\hat{r}_E \cdot \hat{s}_E = \cos 37.64° = 0.792$]. Similar to the central-beam $\mathbf{E} \perp \mathbf{K}$ polarization case [Fig. 3(a)], the
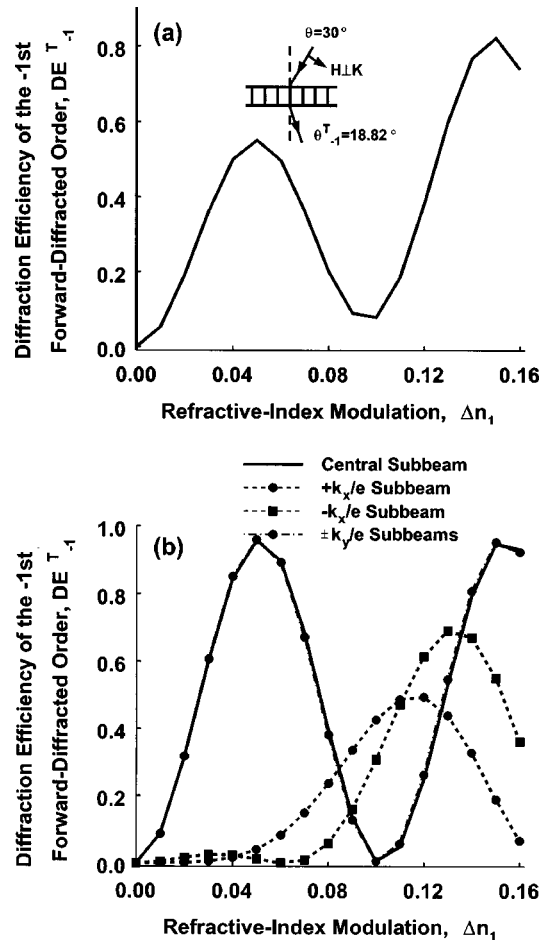

Fig. 5. Diffraction efficiencies of the −1st forward-diffracted order of an unslanted VG for (a) a converging–diverging spherical Gaussian beam and (b) its corresponding five major subbeams as a function of the refractive-index modulation for central-beam $\mathbf{H} \perp \mathbf{K}$ polarization case.
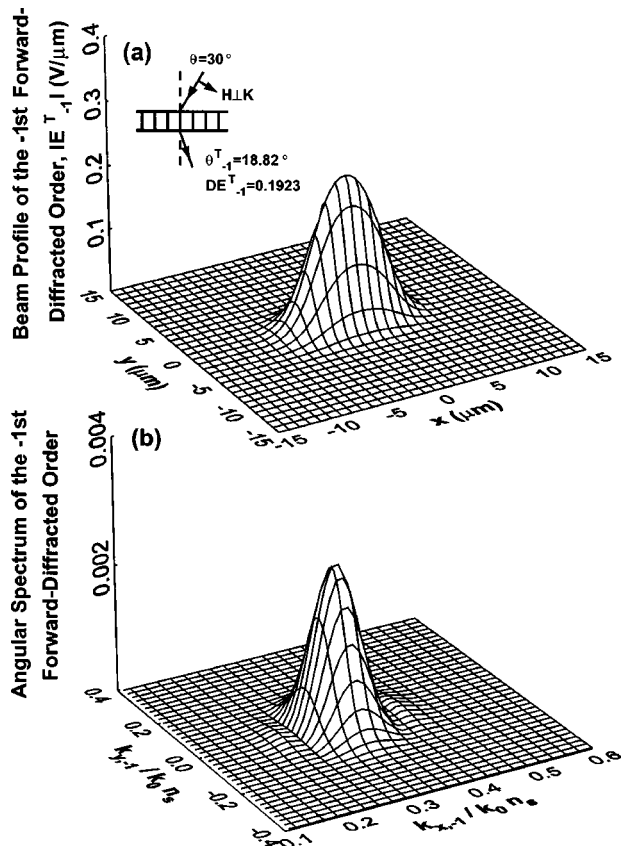
Fig. 6.   (a) 3-D beam profile at $z=10$ μm and (b) its corresponding angular spectrum of the -1th forward-diffracted order of an unslanted VG for the central-beam $\mathbf{H} \perp \mathbf{K}$ polarization case with grating $\Delta n_1 = 0.02$.

diffraction efficiency of the central-beam $\mathbf{H} \perp \mathbf{K}$ polarization case [Fig. 5(a)] increases as the refractive-index modulation increases and approaches the central-beam result [solid curve in Fig. 5(b)]. Furthermore, the diffraction characteristics of the five major subbeams for the central-beam $\mathbf{H} \perp \mathbf{K}$ polarization case [Fig. 5(b)] are similar to those of the central-beam $\mathbf{E} \perp \mathbf{K}$ polarization case [Fig. 3(b)]. For small values of Δn_1, the diffraction efficiencies for both $\pm k_x/e$ subbeams are much smaller than those of the central subbeam. However, the diffraction efficiencies of both $\pm k_y/e$ subbeams are identical to each other and are close to those of the central subbeam.

The 3-D beam profile at $z=10$ μm and its corresponding angular spectrum of the -1st forward-diffracted order for the central-beam $\mathbf{H} \perp \mathbf{K}$ polarization case with grating $\Delta n_1 = 0.02$ are summarized in Fig. 6. Similar to the central-beam $\mathbf{E} \perp \mathbf{K}$ polarization case, the beam profile of the -1st forward-diffracted order is also not a Gaussian profile [Fig. 6(a)], and its angular spectrum is also centered at $k_{x,-1}/k_0 n_s = 0.323$ and $k_{y,-1}/k_0 n_s = 0$ [Fig. 6(b)]. In addition, the subbeams of the -1st forward-diffracted beam are linearly polarized and elliptically polarized as $k_{y,-1}=0$ and $k_{y,-1} \neq 0$, respectively. For $\Delta n_1 = 0.02$, the corresponding diffraction efficiency of the central-beam $\mathbf{H} \perp \mathbf{K}$ polarization case is 19.23%, which is smaller than that of the central-beam $\mathbf{E} \perp \mathbf{K}$ polarization case that is in agreement with the expectation of Kogelnik's analysis.[35]

B. Slanted Volume Gratings

For the case of a slanted VG, the grating period and the slant angle are designed to provide a 45° [i.e., $\theta_{-1}^T = 45°$ (with respect to the $+z$ axis in a counterclockwise direction)] forward-diffraction angle of the -1st propagating order to achieve multiple total internal reflections within the substrate for a substrate-mode optical interconnect as the incident beam is normally incident on the VG (i.e., $\theta = \phi = 0°$). Therefore, based on the first-order Bragg condition, the grating period and the slant angle of this slanted VG are $\Lambda = 711.37$ nm and $\phi_g = 113.47°$, respectively.

1. $\mathbf{E} \perp \mathbf{K}$ *Polarization*

Figure 7 shows the diffraction efficiencies DE_{-1}^T for the converging–diverging spherical Gaussian beam and its corresponding five major subbeams as a function of Δn_1. As is shown in Fig. 7(a), the period of DE_{-1}^T is $\Delta n_1^p = 0.07$, which is close to the value estimated by Eq. (18) for $\theta_{\mathrm{ins}} = 0°$ and $\hat{r}_E \cdot \hat{s}_E = 1$. Comparing Figs. 3 and 7, the diffraction characteristics of a slanted VG resemble those of an unslanted VG for the central-beam $\mathbf{E} \perp \mathbf{K}$ polarization case. The diffraction efficiency of the central-beam $\mathbf{E} \perp \mathbf{K}$ polarization case for a slanted VG increases as the
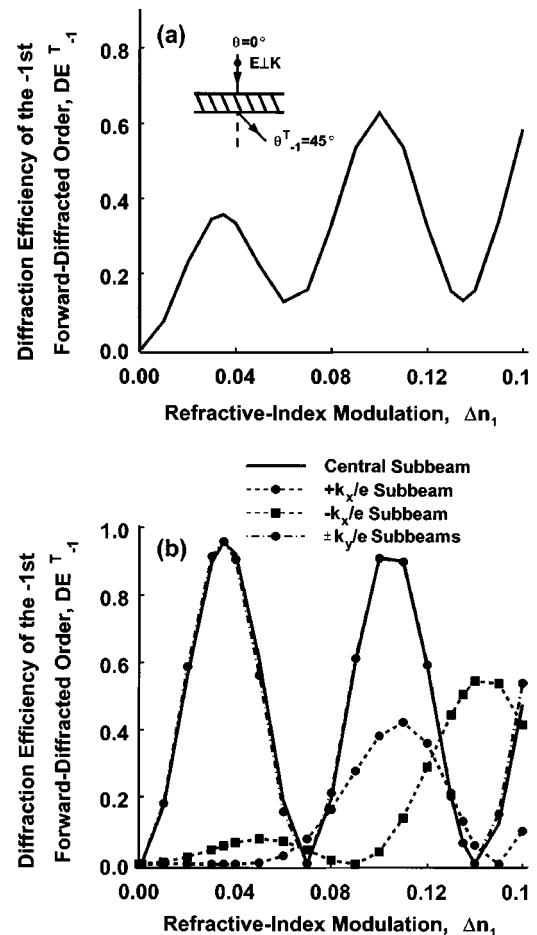

Fig. 7.   Diffraction efficiencies of the -1st forward-diffracted order of a slanted VG designed to support a substrate-mode optical interconnect for (a) a converging–diverging spherical Gaussian beam and (b) its corresponding five major subbeams as a function of the refractive-index modulation for the central-beam $\mathbf{E} \perp \mathbf{K}$ polarization case.
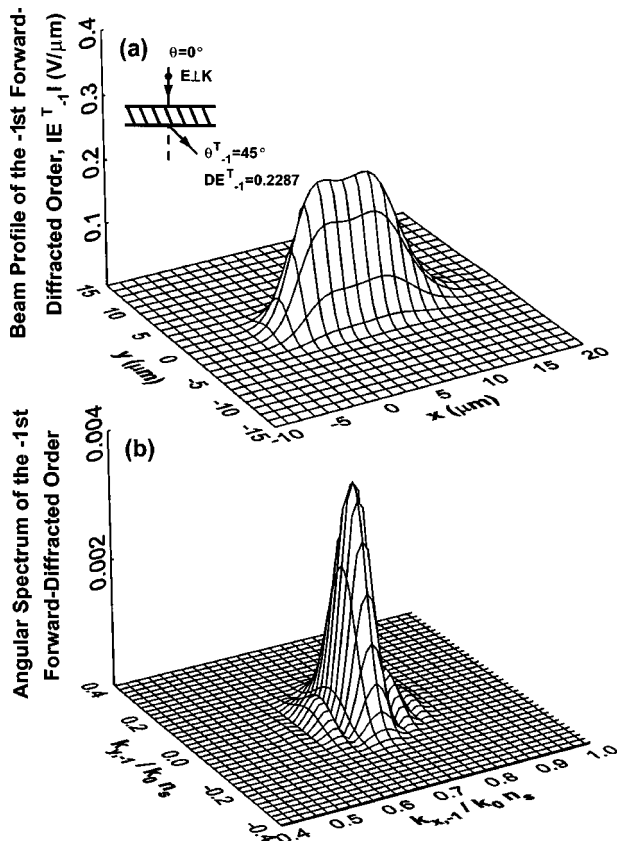
Fig. 8. (a) 3-D beam profile at $z=10$ μm and (b) its correspond-ing angular spectrum of the -1st forward-diffracted order of a slanted VG designed to support a substrate-mode optical inter-connect for the central-beam $\mathbf{E} \perp \mathbf{K}$ polarization case with grat-ing $\Delta n_1 = 0.02$.

refractive-index modulation increases [Fig. 7(a)] and ap-proaches the central-beam result [solid curve in Fig. 7(b)]. Furthermore, as is shown in Fig. 7(b), the diffraction effi-ciencies for both $\pm k_x/e$ subbeams are much smaller than those of the central subbeam for small values of Δn_1, and the diffraction efficiencies of both $\pm k_y/e$ subbeams are identical to each other and are close to those of the central subbeam.

Furthermore, Fig. 8 shows the 3-D beam profile at $z = 10$ μm and its corresponding angular spectrum of the -1st forward-diffracted order for the central-beam $\mathbf{E} \perp \mathbf{K}$ polarization case with grating $\Delta n_1 = 0.02$. Similar to an unslanted VG [Fig. 4(a)], the spherical Gaussian beam is also distorted by a slanted VG [Fig. 8(a)]. On the other hand, as is shown in Fig. 8(b), the angular spectrum of the -1st forward-diffracted order is centered at $k_{x,-1}/k_0 n_s = 0.707$ and $k_{y,-1}/k_0 n_s = 0$. That is, the diffracted angle of the -1st forward-diffracted order is $\theta_{-1}^T = 45°$ on the $x-z$ plane, which satisfies the design of 45° forward-diffraction angle to achieve the substrate-mode optical in-terconnect. The subbeams of the -1st forward-diffracted beam are linearly polarized and elliptically polarized for $k_{y,-1} = 0$ and $k_{y,-1} \neq 0$, respectively, outcomes which are consistent with the unslanted VG results. Also, the corre-sponding coupling efficiency of the substrate-mode optical interconnect is 22.87% for the central-beam $\mathbf{E} \perp \mathbf{K}$ polar-ization case. As is shown in Fig. 7(a), a higher coupling

efficiency for the central-beam $\mathbf{E} \perp \mathbf{K}$ polarization case can be obtained by increasing the refractive-index modu-lation. For example, for $\Delta n_1 = 0.1$ the coupling efficiency can achieve 62.99% for a converging–diverging spherical Gaussian beam with a beam radius of $w_{0x'} = w_{0y'} = 2$ μm (i.e., with a beam diameter of 4 μm). However, in many practical applications the beam diameter of a spherical Gaussian beam might be ~10 μm, and therefore the cor-responding coupling efficiency of the central-beam $\mathbf{E} \perp \mathbf{K}$ polarization case for this substrate-mode optical intercon-nect can be up to 86.62% for $\Delta n_1 = 0.1$.

2. $\mathbf{H} \perp \mathbf{K}$ *Polarization*

Similarly, the diffraction characteristics of a substrate-mode optical interconnect for the central-beam $\mathbf{H} \perp \mathbf{K}$ po-larization case with respect to Δn_1 are presented in Fig. 9. As is shown in Fig. 9(a), the value of Δn_1^p is 0.10 [close to the value estimated by Eq. (18) with $\theta_{\text{ins}} = 0°$ and $\hat{r}_E \cdot \hat{s}_E = \cos 45° = 0.707$], and the diffraction efficiency increases as Δn_1 increases and approaches the central-beam result, which is consistent with both unslanted (Figs. 3 and 5) and slanted VGs (Fig. 7). Based on $\Delta n_1 = 0.02$ (i.e., Du-Pont's OmniDex613 photopolymer), the 3-D beam profile
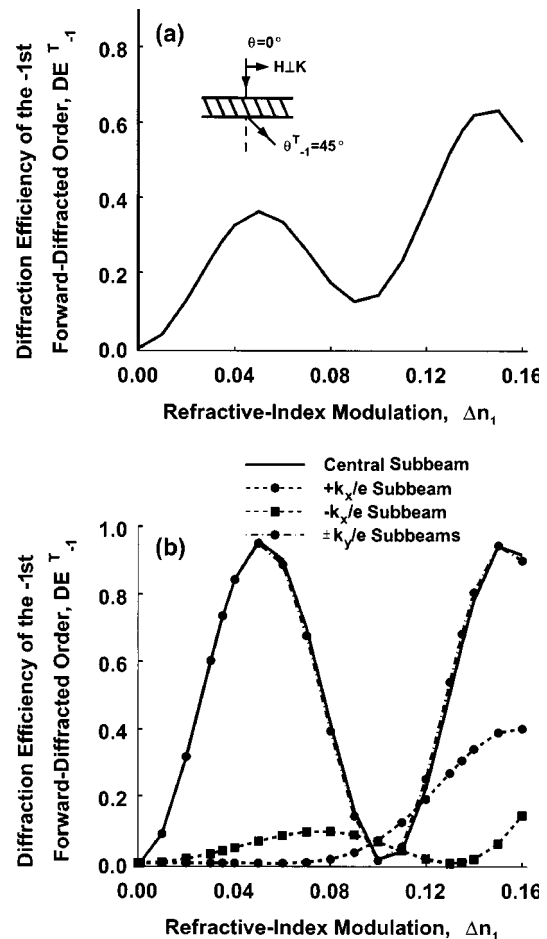

Fig. 9. Diffraction efficiencies of the -1st forward-diffracted or-der of a slanted VG designed to support a substrate-mode optical interconnect for (a) a converging–diverging spherical Gaussian beam and (b) its corresponding five major subbeams as a function of the refractive-index modulation for the central-beam $\mathbf{H} \perp \mathbf{K}$ po-larization case.
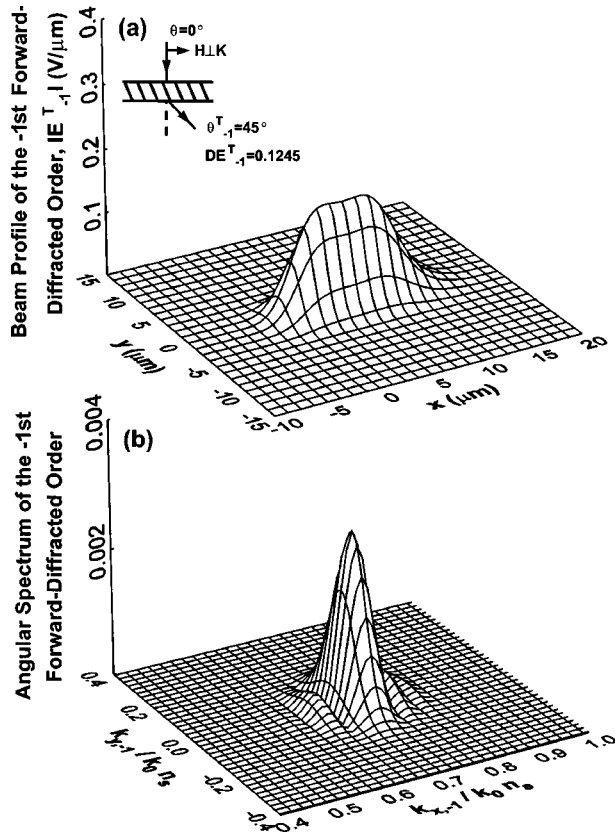
Fig. 10. (a) 3-D beam profile at $z = 10$ μm and (b) its corresponding angular spectrum of the -1st forward-diffracted order of a slanted VG designed to support a substrate-mode optical interconnect for the central-beam $\mathbf{H} \perp \mathbf{K}$ polarization case with grating $\Delta n_1 = 0.02$.

at $z = 10$ μm and its corresponding angular spectrum of the -1st forward-diffracted order for the central-beam $\mathbf{H} \perp \mathbf{K}$ polarization case are presented in Fig. 10. As is shown in Fig. 10, the beam profile of the -1st forward-diffracted order is no longer Gaussian; its angular spectrum is centered at $k_{x,-1}/k_0 n_s = 0.707$ and $k_{y,-1}/k_0 n_s = 0$ (i.e., the corresponding diffracted angle is $\theta_{-1}^T = 45°$), and its corresponding subbeams are linearly polarized and elliptically polarized for $k_{y,-1} = 0$ and $k_{y,-1} \neq 0$, respectively. The coupling efficiency of this substrate-mode optical interconnect for the central-beam $\mathbf{H} \perp \mathbf{K}$ polarization case is 12.45%, which is smaller than that of the central-beam $\mathbf{E} \perp \mathbf{K}$ polarization case (22.87%), which is in agreement with Kogelnik's analysis.[35] Similar to the central-beam $\mathbf{E} \perp \mathbf{K}$ polarization case, the coupling efficiency for the central-beam $\mathbf{H} \perp \mathbf{K}$ polarization case can also increase to a higher coupling efficiency of 63.28% as the refractive-index modulation increases to $\Delta n_1 = 0.15$. Furthermore, for a spherical Gaussian beam with a beam diameter of 10 μm, the coupling efficiency of the $\mathbf{H} \perp \mathbf{K}$ polarization case can reach 89.06% for $\Delta n_1 = 0.15$.

4. SUMMARY AND DISCUSSION

A three-dimensional (3-D) finite-beam (FB) rigorous coupled-wave analysis (RCWA) based on the conventional 3-D RCWA in conjunction with a two-dimensional (2-D)

plane-wave decomposition (PWD) is presented to analyze rigorously the 3-D converging–diverging spherical Gaussian beam diffraction by a volume grating (VG). The diffraction characteristics, including the diffraction efficiencies and the diffracted-beam profiles for both unslanted VGs and slanted VGs, which are designed for substrate-mode optical interconnects, and for two linear polarizations of the central portion of the Gaussian beam for $\mathbf{E} \perp \mathbf{K}$ and $\mathbf{H} \perp \mathbf{K}$, are investigated. In general, the diffraction efficiencies of converging–diverging spherical Gaussian beams in both the central-beam $\mathbf{E} \perp \mathbf{K}$ polarization case and the central-beam $\mathbf{H} \perp \mathbf{K}$ polarization case diffracted by both unslanted and slanted VGs increase and approach the central-beam results as the refractive-index modulation increases. The period of the variation of the diffraction efficiency with respect to the refractive-index modulation of a converging–diverging spherical Gaussian beam is close to the value estimated by Kogelnik's analysis. In addition, according to the numerical results of diffraction efficiencies for five major subbeams, including the central subbeam, the $\pm k_x/e$ subbeams, and the $\pm k_y/e$ subbeams, the diffraction efficiencies of both $\pm k_x/e$ subbeams are much smaller than those of the central subbeam for the small refractive-index modulation ($\Delta n_1 \leqslant 0.03$). However, as the refractive-index modulation increases, the diffraction efficiencies of both $\pm k_x/e$ subbeams increase and become comparable with those of the central subbeam. On the other hand, the diffraction efficiencies of both $\pm k_y/e$ subbeams are identical to each other and are close to those of the central subbeam. In general, the diffracted-beam profiles are shown to be no longer Gaussian; i.e., the diffracted beams are distorted by the VGs. Furthermore, the subbeams of the -1st forward-diffracted beams are linearly polarized and elliptically polarized as $k_{y,-1} = 0$ and $k_{y,-1} \neq 0$, respectively.

For the application of a substrate-mode optical interconnect realized by a slanted VG, the coupling efficiency for central-beam $\mathbf{E} \perp \mathbf{K}$ polarization case increases from 22.85% to 62.99% as the refractive-index modulation increases from $\Delta n_1 = 0.02$ to $\Delta n_1 = 0.1$ for a beam diameter of 4 μm. On the other hand, for the central-beam $\mathbf{H} \perp \mathbf{K}$ polarization case, the coupling efficiency of the substrate-mode optical interconnect increases from 12.45% to 63.28% as the refractive-index modulation increases from $\Delta n_1 = 0.02$ to $\Delta n_1 = 0.15$ for a beam diameter of 4 μm. However, for the practical case of a beam diameter of 10 μm, the coupling efficiency for both the central-beam $\mathbf{E} \perp \mathbf{K}$ polarization case and the central-beam $\mathbf{H} \perp \mathbf{K}$ polarization case are 86.62% for $\Delta n_1 = 0.1$ and 89.06% for $\Delta n_1 = 0.15$, respectively. Finally, it is worth mentioning that, although the analysis of conical diffraction for VGs in this paper only emphasized a 3-D converging–diverging spherical Gaussian beam [i.e., $w_{0x'}(z' = 0) = w_{0y'}(z' = 0)$, defined in Eq. (3)], it can be extended to a general 3-D converging–diverging elliptical Gaussian beam of TEM_{00} mode [i.e., $w_{0x'}(z' = 0) \neq w_{0y'}(z' = 0)$, defined in Eq. (3)] as well as of higher orders with appropriate changes in the amplitudes and phase factors. Furthermore, the present method of 3-D FB RCWA can be used for the diffraction analysis of a surface-relief grating illuminated by a finite incident

beam (such as a general 3-D converging–diverging elliptical Gaussian beam) at an arbitrary incidence angle, at an arbitrary azimuthal angle, and with any linear polarization.

APPENDIX A: DEFINITIONS OF THE CENTRAL SUBBEAM, THE $\pm k_x/e$ SUBBEAMS, AND THE $\pm k_y/e$ SUBBEAMS

To define the central subbeam, the $\pm k_x/e$ subbeams, and the $\pm k_y/e$ subbeams, a normally incident beam focused on a VG is considered, and therefore the beam-coordinate system (x',y',z') is identical to the VG coordinate system (x,y,z) (Fig. 1). According to Eqs. (2)–(5), the amplitude of the incident filed at $z=0$ (i.e., the interface between the grating and the incident region) can be expressed as

$$E^{\text{inc}} = \exp\left\{ -\left[\left(\frac{x}{w_{0x}} \right)^2 + \left(\frac{y}{w_{0y}} \right)^2 \right] \right\}, \qquad \text{(A1)}$$

where w_{0x} and w_{0y} are the beam radii of the incident beam at the beam waist along the x and the y directions, respectively. By application of the 2-D discrete Fourier transform, the angular spectrum of Eq. (A1) is analytic and is given by

$$F^{\text{inc}}(k_x,k_y) = \frac{w_{0x}w_{0y}}{4\pi} \exp\left\{ -\left[\left(\frac{w_{0x}}{2}k_x \right)^2 + \left(\frac{w_{0y}}{2}k_y \right)^2 \right] \right\}, \qquad \text{(A2)}$$

where k_x and k_y are the components of a wave vector along the x and y directions, respectively, for a specific subbeam. As a result, the corresponding z wave vector component is $k_z = (k_0^2 n_I^2 - k_x^2 - k_y^2)^{1/2}$. As shown in Eq. (A2), the maximum value of the angular spectrum occurs at $k_x=0$ and $k_y=0$, which corresponds to the central subbeam. On the other hand, for the subbeams of $k_y=0$, the angular spectrum falls to $1/e$ of its amplitude value of the central beam at $k_x=2/w_{0x}$ and $k_x=-2/w_{0x}$, which are defined as the $+k_x/e$ subbeam and the $-k_x/e$ subbeam, respectively. Similarly, the $+k_y/e$ subbeam and the $-k_y/e$ subbeam correspond to $k_y=2/w_{0y}$ and $k_y=-2/w_{0y}$, respectively, as $k_x=0$. In summary, the wave vectors of the five major subbeams of a normally incident Gaussian beam can be represented for the central subbeam as

$$\mathbf{k} = k_0 n_I \hat{z}, \qquad \text{(A3)}$$

for the $\pm k_x/e$ subbeam as

$$\mathbf{k} = \pm \frac{2}{w_{0x}} \hat{x} + \left[k_0^2 n_I^2 - \left(\frac{2}{w_{0x}} \right)^2 \right]^{1/2} \hat{z}, \qquad \text{(A4)}$$

and for the $\pm k_y/e$ subbeams as

$$\mathbf{k} = \pm \frac{2}{w_{0y}} \hat{y} + \left[k_0^2 n_I^2 - \left(\frac{2}{w_{0y}} \right)^2 \right]^{1/2} \hat{z}. \qquad \text{(A5)}$$

Furthermore, for a general case of an obliquely incident Gaussian beam at an arbitrary incidence angle θ and at an arbitrary azimuthal angle ϕ (Fig. 1), the corresponding wave vectors, $\mathbf{k}'$ of the five major subbeams of an obliquely incident Gaussian beam can be calculated based on those of a normally incident Gaussian beam according to

$$\mathbf{k}' = \bar{\bar{\mathbf{R}}}_\theta \bar{\bar{\mathbf{R}}}_\phi \mathbf{k}, \qquad \text{(A6)}$$

where

$$\bar{\bar{\mathbf{R}}}_\theta = \begin{bmatrix} \cos\theta & 0 & \sin\theta \\ 0 & 1 & 0 \\ -\sin\theta & 0 & \cos\theta \end{bmatrix}, \qquad \text{(A7)}$$

$$\bar{\bar{\mathbf{R}}}_\phi = \begin{bmatrix} \cos\phi & \sin\phi & 0 \\ -\sin\phi & \cos\phi & 0 \\ 0 & 0 & 1 \end{bmatrix}. \qquad \text{(A8)}$$

REFERENCES

1. J.-H. Yeh and R. K. Kostuk, "Substrate-mode holograms used in optical interconnects: design issues," Appl. Opt. **34**, 3152–3164 (1995).
2. J.-H. Yeh and R. K. Kostuk, "Free-space holographic optical interconnects for board-to-board and chip-to-chip interconnects," Opt. Lett. **21**, 1274–1276 (1996).
3. T. Tanaka, H. Takahashi, Y. Hibino, T. Hashimoto, A. Himeno, Y. Yamada, and Y. Tohmori, "Hybrid external cavity lasers composed of spot-size converter integrated LDs and UV written Bragg grating in a planar lightwave circuit on Si," IEICE Trans. Electron. **E83-C**, 875–883 (2000).
4. S. M. Schultz, E. N. Glytsis, and T. K. Gaylord, "Design, fabrication, and performance of preferential-order volume grating waveguide couplers," Appl. Opt. **39**, 1223–1232 (2000).
5. R. A. Villalaz, E. N. Glytsis, and T. K. Gaylord, "Volume grating couplers: polarization and loss effect," Appl. Opt. **41**, 5223–5229 (2002).
6. S.-D. Wu and E. N. Glytsis, "Volume holographic grating couplers: rigorous analysis using the finite-difference frequency-domain method," Appl. Opt. **43**, 1009–1023 (2004).
7. B. Wang, J. Jiang, and G. P. Nordin, "Compact slanted grating couplers," Opt. Express **12**, 3313–3326 (2004).
8. S. L. Chuang and J. A. Kong, "Wave scattering from a periodic dielectric surface for a general angle of incidence," Radio Sci. **17**, 545–557 (1982).
9. M. G. Moharam and T. K. Gaylord, "Three-dimensional vector coupled-wave analysis of planar-grating diffraction," J. Opt. Soc. Am. **73**, 1105–1112 (1983).
10. M. G. Moharam, E. B. Grann, D. A. Pommet, and T. K. Gaylord, "Formulation for stable and efficient implementation of the rigorous coupled-wave analysis of binary gratings," J. Opt. Soc. Am. A **12**, 1068–1076 (1995).
11. E. Popov and L. Mashev, "Conical diffraction mounting

generalization of a rigorous differential method," J. Opt. **17**, 175–180 (1986).

12. S. D. Gupta, "Theoretical study of plasma resonance absorption in conical diffraction," J. Opt. Soc. Am. B **4**, 1893–1898 (1987).

13. R. A. Depine, "Conformal mapping method for finitely conducting diffraction gratings in conical mountings," Optik (Stuttgart) **81**, 95–102 (1989).

14. M. Gigli and R. A. Depine, "Conical diffraction from uniaxial gratings," J. Mod. Opt. **42**, 1281–1299 (1995).

15. M. Abe and A. Koshiba, "Three-dimensional diffraction analysis of dielectric surface-relief gratings," J. Opt. Soc. Am. A **11**, 2038–2044 (1994).

16. P. Cornet, J. Chandezon, and C. Faure, "Conical diffraction of a plane-wave by an inclined parallel-plate grating," J. Opt. Soc. Am. A **14**, 437–449 (1997).

17. M. Ohki, H. Tateno, and S. Kozaki, "T-matrix analysis of the electromagnetic wave diffraction from a metallic Fourier grating for an arbitrary incidence and polarization," Int. J. Electron. **85**, 787–796 (1998).

18. M. G. Moharam, T. K. Gaylord, and R. Magnusson, "Bragg diffraction of finite beams by thick gratings," J. Opt. Soc. Am. **70**, 300–304 (1980).

19. G. Notni and R. Kowarschik, "Simultaneous diffraction of two finite waves at a nonuniform mixed dynamic transmission grating," J. Opt. Soc. Am. A **7**, 1475–1482 (1990).

20. P. Boffi, J. Osmond, D. Piccinin, M. C. Ubaldi, and M. Martinelli, "Diffraction of optical communication Gaussian beams by volume gratings: comparison of simulations and experimental results," Appl. Opt. **43**, 3854–3865 (2004).

21. R.-S. Chu and T. Tamir, "Bragg diffraction of Gaussian beams by periodically modulated media," J. Opt. Soc. Am. **66**, 220–226 (1976).

22. R.-S. Chu and T. Tamir, "Diffraction of Gaussian beams by periodically modulated media for incidence close to a Bragg angle," J. Opt. Soc. Am. **66**, 1438–1440 (1976).

23. B. Benlarbi, P. St. J. Russell, and L. Solymar, "Diffraction of a Gaussian beam incident upon a thick phase grating," Int. J. Electron. **52**, 209–216 (1982).

24. B. Benlarbi, P. St. J. Russell, and L. Solymar, "Bragg diffraction of Gaussian beams by thick gratings: numerical evaluations by plane-wave decomposition," Appl. Phys. B: Photophys. Laser Chem. **28**, 383–390 (1982).

25. Em. E. Kriezis, P. K. Pandelakis, and A. G. Papagiannakis, "Diffraction of a Gaussian beam from a periodic planar screen," J. Opt. Soc. Am. A **11**, 630–636 (1994).

26. M. D. McNeill and T.-C. Poon, "Gaussian-beam profile shaping by acousto-optic Bragg diffraction," Appl. Opt. **33**, 4508–4514 (1994).

27. D. C. Skigin and R. A. Depine, "Model theory for diffraction from a dielectric aperture with arbitrarily shaped corrugations," Opt. Commun. **149**, 117–126 (1998).

28. O. Mata-Mendez and F. Chavez-Rivas, "Diffraction of a Gaussian and Hermite Gaussian beams by finite gratings," J. Opt. Soc. Am. A **18**, 537–545 (2001).

29. J. Sumaya-Martines, O. Mata-Mendez, and F. Chavez-Rivas, "Rigorous theory of the diffraction of Gaussian beams by finite gratings: TE polarizations," J. Opt. Soc. Am. A **20**, 827–835 (2003).

30. A. E. Siegman, "Bragg diffraction of a Gaussian beam by a crossed-Gaussian volume grating," J. Opt. Soc. Am. **67**, 545–550 (1977).

31. A. Y. Hamad and J. P. Wicksted, "Volume grating produced by intersecting Gaussian beams in an absorbing medium: a Bragg diffraction model," Opt. Commun. **138**, 354–364 (1997).

32. M. G. Moharam, T. K. Gaylord, and R. Magnusson, "Diffraction characteristics of three-dimensional crossed-beam volume gratings," J. Opt. Soc. Am. **70**, 437–442 (1980).

33. M. R. Wang, "Analysis and observation of finite beam Bragg diffraction by a thick planar phase grating," Appl. Opt. **35**, 582–592 (1996).

34. G. D. Landry and T. A. Maldonado, "Gaussian beam transmission and reflection from a general anisotropic multilayer structure," Appl. Opt. **35**, 5870–5879 (1996).

35. H. Kogelnik, "Coupled-wave theory for thick hologram gratings," Bell Syst. Tech. J. **48**, 2909–2947 (1969).

36. S.-D. Wu and E. N. Glytsis, "Holographic grating formation in photopolymers: analysis and experimental results based on a nonlocal diffusion model and rigorous coupled-wave analysis," J. Opt. Soc. Am. B **20**, 1177–1188 (2003).

37. S.-D. Wu and E. N. Glytsis, "Characteristics of DuPont photopolymers for slanted holographic grating formations," J. Opt. Soc. Am. B **21**, 1722–1731 (2004).